JOURNAL OF SPACECRAFT AND ROCKETS
Vol. 52, No. 2, March–April 2015

Spacecraft Propulsion Using Angular Momentum Transfer Based on Gravity Gradient Effects

Brian Lynch*
Queen's University, Kingston, Ontario K7L 3N6, Canada
and
Alex Ellery†
Carleton University, Ottawa, Ontario K1S 5B6, Canada

DOI: 10.2514/1.A32924

Typical spacecraft propulsion systems depend upon the transfer of linear momentum through the expulsion of propellant using rocket motors or ion thrusters. This paper presents a method of spacecraft propulsion in which rotational angular momentum is transferred to orbital angular momentum due to the influence of gravity gradient effects. By applying torque to maintain a specific orientation with respect to the gravity gradient, the spacecraft orbital angular momentum is increased or decreased. If momentum wheels or control moment gyroscopes are used, no propellant is required and orbital maneuvers may be performed using solely electrical power. The equations of motion are presented along with analysis of the resulting change in orbital elements, demonstrating the relationship between spacecraft orientation and effective propulsive thrust. Simulation of the equations of motion is used to demonstrate the performance of the proposed technique and is verified by comparing results using both Lagrange dynamics and Newton–Euler dynamics. Although the resulting effects of this approach are small in comparison with conventional propulsion methods, it may be useful in applications such as exploration of asteroids and small moons, deorbiting of decommissioned satellites, or simply to reduce the requirements of a primary propulsion system.

Nomenclature

a	=	orbit semimajor axis, m
d_M,d_m	=	radial distance between fixed central body and mass M, m, m
E	=	orbital energy, J
e	=	orbit eccentricity
$\boldsymbol{F}_M$, $\boldsymbol{F}_m$	=	gravity forces acting on mass M, m
F_r, F_θ	=	net force in radial and tangential directions, N
G	=	universal gravitational constant, N $\cdot$ m^2/kg^2
H	=	angular momentum, N $\cdot$ ms
h	=	specific angular momentum, m^2/s
I_ϕ	=	spacecraft mass moment of inertia, kg $\cdot$ m^2
L	=	simplified spacecraft length, m
M	=	mass of larger spacecraft tip, kg
M_T	=	total spacecraft mass, kg
m	=	mass of smaller spacecraft tip, kg
P_ϕ	=	power, W
p	=	orbit semilatus rectum, m
Q_r, Q_θ	=	generalized force in radial and tangential directions, N
Q_ϕ	=	generalized moment about vertical axis, N $\cdot$ m
r	=	radial distance between central body and spacecraft center of mass, m
r_a	=	orbit apoapsis, m
r_M, r_m	=	radial distance between free central body and mass M, m, m
r_p	=	orbit periapsis, m
T	=	total kinetic energy, J
$\boldsymbol{u}_M$, $\boldsymbol{u}_m$	=	unit vector from central body to mass M, m
V	=	total potential energy, J
v	=	spacecraft speed, m/s
v_M, v_m	=	speed of mass M, m, m/s
x	=	x coordinate of spacecraft, m
x_{CB}	=	x coordinate of central body, m
x_M, x_m	=	x coordinate of mass M, m, m
y	=	y coordinate of spacecraft, m
y_{CB}	=	y coordinate of central body, m
y_M, y_m	=	y coordinate of mass M, m, m
z, z_a	=	normalized apsis and apoapsis parameters
z_p	=	normalized periapsis parameter
α	=	spacecraft orientation relative to zenith, rad
β	=	normalized radial parameter
γ	=	flight-path angle, rad
Δ	=	normalized thrust parameter
δ_M, δ_m	=	normalized radial distance between central body and mass M, m
ε	=	mass distribution ratio
ζ	=	apsis orientation angle, rad
ζ_a	=	apoapsis orientation angle, rad
ζ_p	=	periapsis orientation angle, rad
η	=	mass distribution parameter
Θ	=	apsis orientation function
θ	=	spacecraft angular position, rad
λ	=	normalized spacecraft length
μ	=	central body gravitation parameter, m^3/s^2
ξ	=	eccentricity orientation angle, rad
ρ	=	normalized eccentricity parameter
σ	=	argument of periapsis orientation angle, rad
ϕ	=	spacecraft orientation relative to inertial space, rad
χ	=	eccentricity orientation function
ψ	=	semimajor axis orientation function
ω	=	argument of periapsis, rad

Received 6 January 2014; revision received 27 June 2014; accepted for publication 25 August 2014; published online 10 December 2014.

*Postdoctoral Fellow, Robert M. Buchan Department of Mining.
†Associate Professor, Department of Mechanical and Aerospace Engineering.

I. Introduction

THE conventional method of propelling a spacecraft is the use of solid or liquid rocket motors, in which the combustion of propellants (fuel and oxidizer) generates hot gases that are channeled through a nozzle and expelled [1]. As the hot gases leave the nozzle at high velocity, thrust is generated, which transfers linear momentum to the spacecraft. Cold gas thrusters generate thrust similarly but by using only a single propellant gas, which is held under pressure and released upon command. Another method that has been studied and

applied is the use of ion thrusters, in which charged particles are accelerated through an electromagnetic field and expelled at high velocity [2–4]. Rocket motors, cold gas thrusters, and ion thrusters all depend upon the transfer of linear momentum between expelled propellant and the spacecraft body.

Although improvements in motor and propellant efficiencies are continually being investigated, high-thrust propulsion using rocket motors or cold gas thrusters necessitates a large mass of propellant carried by the spacecraft. On the other hand, ion thrusters provide low thrust but necessitate a much lower total propellant mass. The impact of the propellant mass requirement upon the overall mission is significant, resulting in large multistage launch vehicles that lift relatively small payloads. Reducing the propellant mass requirements allows a larger payload mass to be carried, which may take the form of additional instruments, safer design margins, longer mission durations, and so on. Therefore, other forms of spacecraft propulsion that do not require propellant mass are attractive and have been given much consideration.

Generating reaction forces between the vehicle and surrounding environment is the most practical method of spacecraft propulsion without consuming propellant. Although the space environment is typically considered empty and therefore unable to provide reaction forces, it is possible to do so by exploiting electromagnetic fields as well as solar wind. Electric current flowing along a tether may be used to generate thrust due to the Lorentz force as it interacts with the magnetic field of a central body [5–7]. This effect has been well studied for use in spacecraft propulsion but requires complex systems to maintain a proper current flow. Solar sails have also been studied extensively, where the pressure of particles emanating from the sun is used to generate propulsive thrust [8,9]. Although the pressure due to solar wind is small, its continuous application upon a large surface area results in significant propulsive effects over time and the system itself is relatively simple. Aerobraking is another example of propellantless propulsion through interactions with the surrounding environment, because the spacecraft is decelerated using aerodynamic drag [10,11]. However, this effect is risky, and may only be used to slow the spacecraft according to the atmospheric conditions of the central body. Similarly, atmospheric drag may be used for steering satellite formations, as studied using ORBCOMM and JC2Sat [12].

Momentum exchange tethers are another method of propelling spacecraft without the use of propellant. The spacecraft (or other payload) is captured and spun at the tip of a tether in orbit around a central body and released at an appropriate point in the trajectory, thus departing with increased or decreased momentum relative to its initial capture point [13–15]. This may be synchronized with the release of another payload in the opposite direction to maintain momentum balance, otherwise the orbit of the tether itself must be boosted appropriately. Momentum exchange tethers are relatively simple systems but require advanced materials and reliable control techniques to maintain a desired tension and spin rate.

The most well-established method of spacecraft propulsion without the use of propellant mass is the use of a gravity-assist maneuver, where the spacecraft is placed upon a hyperbolic orbit around a central body and exchanges momentum as it passes. This method has been relied upon for most missions in which spacecraft are sent to the outer planets of the solar system, such as Voyagers 1 and 2 and Pioneer 11 [16]. In a gravity-assist maneuver, the spacecraft approaches the central body at an initial speed and departs the central body at the same speed but with a new direction due to the exchange of momentum. Although there is no change in speed relative to the central body, there is a change in speed relative to the sun (or other celestial body around which the central body orbits). Therefore, the gravity-assist maneuver allows the spacecraft to achieve a propulsive effect relative to its overall mission trajectory.

Another effect experienced by spacecraft is the gravitational gradient, which manifests as a net moment due to the difference in strength in gravity at various points on the vehicle. Elements of the vehicle closer to the central body are subject to larger gravity forces than those further away, and there exist one or more stable and unstable equilibrium orientations toward which the spacecraft tends to rotate. Although this effect is typically considered a perturbation that must be counteracted using the spacecraft attitude control system [17], it is also possible to use the gravitational gradient to generate propulsive thrust, as will be shown in this paper.

The method of spacecraft propulsion proposed here consists of orienting the spacecraft at a specific angle with respect to the line of action of the gravity force (or zenith) upon the spacecraft center of mass. Because of the gravitational gradient effect and distribution of mass across the volume of the vehicle, a component of gravity force arises in the tangential direction with respect to the zenith. This tangential component of force creates a propulsive effect, which may be used to increase or decrease the velocity of the spacecraft, and hence raise or lower the orbit, depending upon the orientation angle. Similar to the gravity-assist maneuver, this method of spacecraft propulsion exchanges linear momentum with the central body. To maintain the specified orientation, the spacecraft must generate torque to counteract the effects of the gravitational gradient using an attitude control system. Angular momentum is then exchanged between the spacecraft and its orbit. Using momentum wheels or control moment gyroscopes, only electrical power is needed to perform the propulsive maneuver instead of propellant.

This method is found to generate relatively small thrust and may not provide the necessary propulsion to meet the orbit maneuver requirements of most missions. However, it may prove useful as an auxiliary propulsion source in applications such as deorbiting satellites at their end of life or boosting low orbits in the presence of perturbations such as atmospheric drag. With the increasing interest in in situ resource utilization for space exploration, the simplicity of this system makes it attractive for use in missions to asteroids or other smaller bodies. A primary propulsion system would still be necessary, but this approach could reduce propellant requirements and increase the mission lifetime.

Although the proposed propulsion method in this paper has been conceived independently by the author, a literature review revealed previous research in which similar techniques are studied. Landis analyzed a dumbbell model spacecraft that oriented itself with respect to the gravity gradient, then extended and retracted to increase orbital energy [18]. Similar methods of altering the orbital parameters based on tether deployment and retraction have also been studied recently by Djebli and Pascal [19]. Although these approaches are entirely valid, the proposed method in this paper requires no retractable tether mechanism and may be applied by any spacecraft with an attitude control system. Watanabe and Nakamura demonstrated the same propulsion technique proposed in this paper and found the same resulting spacecraft orientation for maximizing thrust [20]. However, their analysis was limited to numerical simulations at a fixed orientation. This paper contributes a more complete analysis of the optimal orientation profiles required to change the spacecraft semimajor axis, eccentricity, apses, and argument of periapsis. Simulation is used to test the proposed techniques and validate assumptions using exaggerated models to amplify the effects, and more realistic cases are also investigated for comparison.

II. Equations of Motion

The equations of motion are determined for a simplified model of the spacecraft, which is composed of a smaller mass m and larger mass M, connected rigidly across a distance L. The ratio of the smaller mass to the total mass of the spacecraft is defined by Eq. (1) and the total mass of the spacecraft is defined by Eq. (2):

$$\varepsilon = \frac{m}{m+M} \tag{1}$$

$$M_T = m + M \tag{2}$$

The position of the central body is assumed to be fixed in inertial space for the majority of analyses, which are performed using equations of motion defined within polar coordinates and determined by Lagrange dynamics. This assumption is shown to be valid by analyzing the system without a fixed central body using equations of

motion defined within Cartesian coordinates and determined by Newton–Euler dynamics.

Figure 1 shows the kinematic model of the spacecraft with respect to the central body (CB) where the spacecraft orientation is defined by the angle α.

A. Lagrange Dynamics

Let r and θ define the position of the spacecraft center of mass in polar coordinates, which may also be described in Cartesian coordinates according to Eq. (3):

$$\begin{bmatrix} x \\ y \end{bmatrix} = \begin{bmatrix} r\cos\theta \\ r\sin\theta \end{bmatrix} \tag{3}$$

The orientation of the spacecraft with respect to the inertial coordinate frame is defined by the angle ϕ and the orientation of the spacecraft with respect to the zenith is α, as defined by

$$\alpha = \phi - \theta \tag{4}$$

Similarly, the positions of masses m and M may be described by Eqs. (5) and (6), respectively:

$$\begin{bmatrix} x_m \\ y_m \end{bmatrix} = \begin{bmatrix} x + (1-\varepsilon)L\cos\phi \\ y + (1-\varepsilon)L\sin\phi \end{bmatrix} \tag{5}$$

$$\begin{bmatrix} x_M \\ y_M \end{bmatrix} = \begin{bmatrix} x - \varepsilon L\cos\phi \\ y - \varepsilon L\sin\phi \end{bmatrix} \tag{6}$$

The distance from the central body to masses m and M may be described by Eqs. (7) and (8), respectively:

$$d_m = \sqrt{r^2 + \varepsilon^2 L^2 - \varepsilon L\cos\alpha} \tag{7}$$

$$d_M = \sqrt{r^2 + (1-\varepsilon)^2 L^2 + (1-\varepsilon)L\cos\alpha} \tag{8}$$

Differentiating by time, the velocities of masses m and M may be described by Eqs. (9) and (10), respectively:

$$\begin{bmatrix} \dot{x}_m \\ \dot{y}_m \end{bmatrix} = \begin{bmatrix} \dot{r}\cos\theta - r\dot{\theta}\sin\theta - (1-\varepsilon)L\dot{\phi}\sin\phi \\ \dot{r}\sin\theta + r\dot{\theta}\cos\theta + (1-\varepsilon)L\dot{\phi}\cos\phi \end{bmatrix} \tag{9}$$

$$\begin{bmatrix} \dot{x}_M \\ \dot{y}_M \end{bmatrix} = \begin{bmatrix} \dot{r}\cos\theta - r\dot{\theta}\sin\theta + \varepsilon L\dot{\phi}\sin\phi \\ \dot{r}\sin\theta + r\dot{\theta}\cos\theta - \varepsilon L\dot{\phi}\cos\phi \end{bmatrix} \tag{10}$$

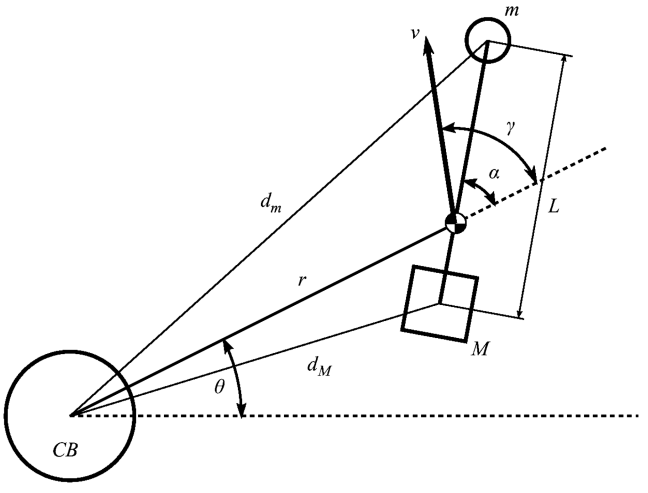

Fig. 1 Kinematic model.

The speeds of masses m and M may then be described by Eqs. (11) and (12), respectively:

$$\begin{aligned} v_m^2 = {} & \dot{r}^2 + r^2\dot{\theta}^2 + (1-\varepsilon)^2 L^2\dot{\phi}^2 \\ & - 2(1-\varepsilon)L\dot{r}\dot{\phi}\sin\alpha \\ & + 2(1-\varepsilon)Lr\dot{\theta}\dot{\phi}\cos\alpha \end{aligned} \tag{11}$$

$$v_M^2 = \dot{r}^2 + r^2\dot{\theta}^2 + \varepsilon^2 L^2\dot{\phi}^2 + 2\varepsilon L\dot{r}\dot{\phi}\sin\alpha - 2\varepsilon Lr\dot{\theta}\dot{\phi}\cos\alpha \tag{12}$$

Equation (13) then defines the kinetic energy of the system T:

$$\begin{aligned} T &= \frac{1}{2}mv_m^2 + \frac{1}{2}Mv_M^2 \\ &= \frac{1}{2}(M+m)(\dot{r}^2 + r^2\dot{\theta} + \varepsilon(1-\varepsilon)L^2\dot{\phi}^2) \end{aligned} \tag{13}$$

Furthermore, Eq. (14) defines the potential energy of the system V, where μ is the gravitational parameter of the central body:

$$V = -\frac{\mu m}{d_m} - \frac{\mu M}{d_M} \tag{14}$$

Using the Lagrange dynamics approach, the equations of motion are defined by Eqs. (15–17), where Q is the generalized force:

$$Q_r = \frac{\mathrm{d}}{\mathrm{d}t}\frac{\partial \dot{T}}{\partial \dot{r}} - \frac{\partial T}{\partial r} + \frac{\partial V}{\partial r} \tag{15}$$

$$Q_\theta = \frac{\mathrm{d}}{\mathrm{d}t}\frac{\partial \dot{T}}{\partial \dot{\theta}} - \frac{\partial T}{\partial \theta} + \frac{\partial V}{\partial \theta} \tag{16}$$

$$Q_\phi = \frac{\mathrm{d}}{\mathrm{d}t}\frac{\partial \dot{T}}{\partial \dot{\phi}} - \frac{\partial T}{\partial \phi} + \frac{\partial V}{\partial \phi} \tag{17}$$

Substitution of the appropriate derivatives results in the equations of motion defined by Eqs. (18–20), where the only external load is the torque due to the attitude control system Q_ϕ:

$$\ddot{r} = r\dot{\theta}^2 - \frac{\mu}{r^2}\beta + \frac{\mu}{r^2}\eta\lambda\Delta\cos\alpha \tag{18}$$

$$\ddot{\theta} = -\frac{2\dot{r}\dot{\theta}}{r} + \frac{\mu}{r^3}\eta\lambda\Delta\sin\alpha \tag{19}$$

$$Q_\phi = M_T\eta\left(L^2\ddot{\phi} + \frac{\mu}{r^2}L\Delta\sin\alpha\right) \tag{20}$$

where $\eta = \varepsilon(1-\varepsilon)$ and $\lambda = L/r$, and the normalized radial and thrust parameters β and Δ are defined by Eqs. (21) and (22), respectively:

$$\beta = \frac{(1-\varepsilon)}{\delta_M^3} + \frac{\varepsilon}{\delta_m^3} \tag{21}$$

$$\Delta = \frac{1}{\delta_M^3} - \frac{1}{\delta_m^3} \tag{22}$$

Equations (23) and (24) define δ_m and δ_M, which are the distances from the central body to the respective mass normalized by the radial distance of the spacecraft r:

$$\delta_m = \frac{d_m}{r} \tag{23}$$

$$\delta_M = \frac{d_M}{r} \tag{24}$$

The parameters β and Δ may be reduced to simplified functions by simplifying the normalized distances δ_m and δ_M according to Eqs. (25) and (26), where the forces from gravity acting on each mass are assumed to be directed along the same line as the zenith with respect to the spacecraft center of mass:

$$\delta_m \approx 1 + (1-\varepsilon)\lambda \cos\alpha \tag{25}$$

$$\delta_M \approx 1 - \varepsilon\lambda \cos\alpha \tag{26}$$

Equations (21) and (22) may be rearranged as shown in Eqs. (27) and (28):

$$\beta = \frac{(1-\varepsilon)\delta_m^3 + \varepsilon\delta_M^3}{\delta_M^3\delta_m^3} \tag{27}$$

$$\Delta = \frac{\delta_m^3 - \delta_M^3}{\delta_M^3\delta_m^3} \tag{28}$$

The cubic terms are then expanded as shown in Eqs. (29) and (30), where $c_\alpha = \cos\alpha$:

$$\begin{aligned}\delta_m^3 &= [1 + (1-\varepsilon)\lambda c_\alpha]^3 \\ &= 1 + 3(1-\varepsilon)\lambda c_\alpha + 3(1-\varepsilon)^2\lambda^2 c_\alpha^2 + (1-\varepsilon)^3\lambda^3 c_\alpha^3\end{aligned} \tag{29}$$

$$\delta_M^3 = (1 + \varepsilon\lambda c_\alpha)^3 \quad = 1 - 3\varepsilon\lambda c_\alpha + 3\varepsilon^2\lambda^2 c_\alpha^2 - \varepsilon^3\lambda^3 c_\alpha^3 \tag{30}$$

Because the length ratio λ is small, some of the terms in Eqs. (29) and (30) may be ignored. However, considering the equations of motion, the Δ term is multiplied by the length ratio, but the β term is not. Equations (29) and (30) are therefore simplified to include only linear terms when substituted into Eq. (28), but both linear and quadratic terms when substituted into Eq. (27).

Substitution of Eqs. (29) and (30) into Eqs. (27) and (28) results in the simplified expressions for β and Δ shown in Eqs. (31) and (32):

$$\begin{aligned}\beta &= \frac{(1-\varepsilon)\delta_m^3 + \varepsilon\delta_M^3}{\delta_M^3\delta_m^3} \\ &\approx \frac{1 + 3(1-2\varepsilon)\lambda c_\alpha + 3(1-3\varepsilon+3\varepsilon^2)\lambda^2 c_\alpha}{1 + 3(1-2\varepsilon)\lambda c_\alpha + 3(1-5\varepsilon+5\varepsilon^2)\lambda^2 c_\alpha} \\ &\approx 1 + 6\eta\lambda^2 c_\alpha\end{aligned} \tag{31}$$

$$\begin{aligned}\Delta &= \frac{\delta_m^3 - \delta_M^3}{\delta_M^3\delta_m^3} \\ &\approx \frac{1 + 3(1-\varepsilon)\lambda c_\alpha - 1 + 3\varepsilon\lambda c_\alpha}{1 + 3(1-2\varepsilon)\lambda c_\alpha} \\ &\approx \frac{3\lambda c_\alpha}{1 + 3(1-2\varepsilon)\lambda c_\alpha} \\ &\approx 3\lambda c_\alpha\end{aligned} \tag{32}$$

Figure 2 shows the actual values of Δ and β compared with the approximations shown in Eqs. (31) and (32). Note that the right-hand plot shows the value of $\beta - 1$ since $\beta \approx 1$.

B. Newton–Euler Dynamics

The gravitational forces acting on masses m and M are defined by Eqs. (33) and (34), respectively:

$$\boldsymbol{F}_m = -\frac{\mu m}{r_m^2}\boldsymbol{u}_m \tag{33}$$

$$\boldsymbol{F}_M = -\frac{\mu M}{r_M^2}\boldsymbol{u}_M \tag{34}$$

where $\boldsymbol{u}_m$ and $\boldsymbol{u}_M$ are unit vectors from the central body to each respective mass defined by Eqs. (35) and (36):

$$\boldsymbol{u}_m = \frac{1}{r_m}\begin{bmatrix} x_m \\ y_m \end{bmatrix} \tag{35}$$

$$\boldsymbol{u}_M = \frac{1}{r_M}\begin{bmatrix} x_M \\ y_M \end{bmatrix} \tag{36}$$

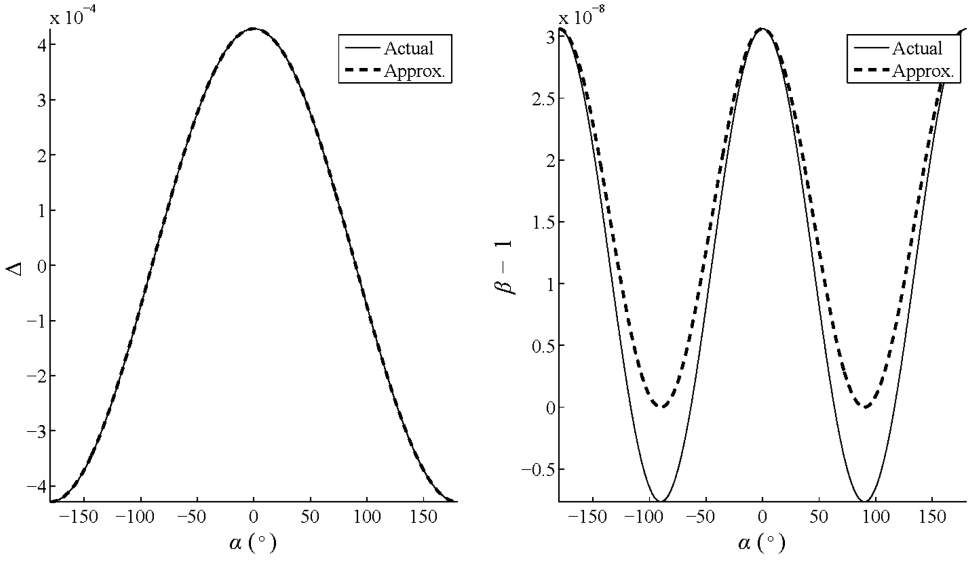

Fig. 2 Comparison of actual and approximated values of Δ and $\beta - 1$.

The distances between each mass and the central body are defined by Eqs. (37) and (38):

$$r_m = \sqrt{[(x_m - x_{\mathrm{CB}})^2 + (y_m - y_{\mathrm{CB}})^2]} \tag{37}$$

$$r_M = \sqrt{[(x_M - x_{\mathrm{CB}})^2 + (y_M - y_{\mathrm{CB}})^2]} \tag{38}$$

The equations of motion for the spacecraft determined through Newton–Euler dynamics are then defined by Eqs. (39) and (40):

$$\ddot{x} = -\frac{\mu\varepsilon}{r_m^3}x_m - \frac{\mu(1-\varepsilon)}{r_M^3}x_M \tag{39}$$

$$\ddot{y} = -\frac{\mu\varepsilon}{r_m^3}y_m - \frac{\mu(1-\varepsilon)}{r_M^3}y_M \tag{40}$$

Similarly, the motion of the central body is defined by Eqs. (41) and (42), where G is the universal gravitational constant:

$$\ddot{x}_{\mathrm{CB}} = \frac{Gm}{r_m^3}x_m + \frac{GM}{r_M^3}x_M \tag{41}$$

$$\ddot{y}_{\mathrm{CB}} = \frac{Gm}{r_m^3}y_m + \frac{GM}{r_M^3}y_M \tag{42}$$

The net gravitational forces upon the spacecraft in polar coordinates are defined by Eqs. (43) and (44):

$$F_r = -\frac{\mu M_T}{r^2}\beta + \frac{\mu M_T}{r^2}\eta\lambda\Delta\cos\alpha \tag{43}$$

$$F_\theta = \frac{\mu M_T}{r^2}\eta\lambda\Delta\sin\alpha \tag{44}$$

Figure 3 shows the gravitational forces acting on each mass and the net gravitational forces in the radial and tangential directions.

III. Orbital Maneuvers

The effect of the spacecraft orientation upon the orbit is investigated by analyzing the semimajor axis a, eccentricity e, apoapsis r_a, periapsis r_p, and argument of periapsis ω. Analysis of the inclination and right ascension of the ascending node will be performed in future research.

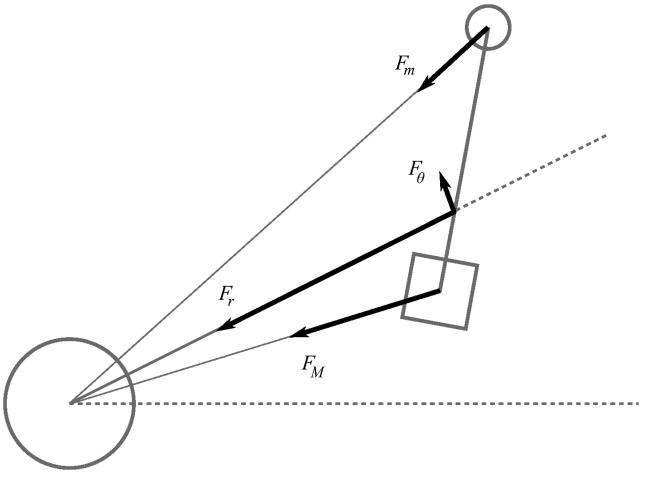

Fig. 3 Gravitational forces.

A. Semimajor Axis

An expression for the semimajor axis is derived from the vis-viva equation [shown in Eq. (45)] and described by Eq. (46), where v is the speed of the spacecraft:

$$v^2 = \mu\left(\frac{2}{r} - \frac{1}{a}\right) \tag{45}$$

$$a = \left(\frac{2}{r} - \frac{v^2}{\mu}\right)^{-1} \tag{46}$$

The semimajor axis defines the total energy of the orbit and must be increased or decreased to raise or lower the orbit. Therefore, the rate of change of the semimajor axis must be found from Eq. (46). First, the speed of the spacecraft is defined according to the polar coordinate frame as shown in Eq. (47):

$$v = \sqrt{\dot{r}^2 + r^2\dot{\theta}^2} \tag{47}$$

Substitution of Eq. (47) within Eq. (46) yields Eq. (48), which is differentiated with respect to time to determine Eq. (49):

$$a = \left(\frac{2}{r} - \frac{\dot{r}^2 + r^2\dot{\theta}^2}{\mu}\right)^{-1} \tag{48}$$

$$\dot{a} = -a^2\left(-\frac{2\dot{r}}{r^2} - \frac{2\dot{r}\,\ddot{r} + 2r\dot{r}\dot{\theta}^2 + 2r^2\dot{\theta}\,\ddot{\theta}}{\mu}\right) \tag{49}$$

The acceleration terms $\ddot{r}$ and $\ddot{\theta}$ are replaced with the respective equations of motion. The resulting relationship for the rate of change of the semimajor axis is defined by Eq. (50):

$$\dot{a} = 2\left(\frac{a}{r}\right)^2[\dot{r}(1-\beta) + \eta\lambda(\dot{r}\cos\alpha + r\dot{\theta}\sin\alpha)\Delta] \tag{50}$$

The simplified expressions for Δ and β may be substituted into Eq. (50) to yield Eq. (51):

$$\begin{aligned}\dot{a} &= 6\left(\frac{a}{r}\right)^2\eta\lambda^2[-2\dot{r}c_\alpha^2 + (\dot{r}c_\alpha + r\dot{\theta}s_\alpha)c_\alpha] \\ &= 6\left(\frac{a}{r}\right)^2\eta\lambda^2(r\dot{\theta}s_\alpha c_\alpha - \dot{r}c_\alpha^2)\end{aligned} \tag{51}$$

Defining the flight-path angle of the spacecraft as γ, which is the angle of the velocity vector with respect to the zenith, the appropriate substitution of the terms $\dot{r} = vc_\gamma$ and $r\dot{\theta} = vs_\gamma$ may be made as shown in Eq. (52):

$$\begin{aligned}\dot{a} &= 6\left(\frac{a}{r}\right)^2\eta\lambda^2 v(s_\gamma s_\alpha c_\alpha - c_\gamma c_\alpha^2) \\ &= 3\left(\frac{a}{r}\right)^2\eta\lambda^2 v[s_\gamma s_{2\alpha} - c_\gamma(c_{2\alpha}+1)] \\ &= 3\left(\frac{a}{r}\right)^2\eta\lambda^2 v(s_\gamma s_{2\alpha} - c_\gamma c_{2\alpha} - c_\gamma) \\ &= 3\left(\frac{a}{r}\right)^2\eta\lambda^2 v[-\cos(2\alpha+\gamma) - \cos\gamma] \\ &= 3\left(\frac{a}{r}\right)^2\eta\lambda^2 v\psi\end{aligned} \tag{52}$$

The parameter ψ defined by Eq. (53) must be analyzed to determine the appropriate value of α for maximizing the propulsive effect to raise or lower the spacecraft orbit:

$$\psi = -\cos(2\alpha + \gamma) - \cos\gamma \tag{53}$$

The maximum and minimum values of ψ are determined according to Eqs. (54–56):

$$\frac{\partial\psi}{\partial\alpha} = 2\,\sin(2\alpha + \gamma)$$
$$0 = \sin(2\alpha + \gamma) \tag{54}$$

$$2\alpha + \gamma = i\pi \qquad i = 0, 1, 2$$
$$\alpha = -\frac{\gamma}{2} + \frac{i\pi}{2} \qquad i = 0, 1, 2 \tag{55}$$

Because the second-order derivative of ψ with respect to α will be negative at a maximum and positive at a minimum, the solutions given by Eq. (55) may be substituted as shown in Eq. (56):

$$\frac{\partial^2\psi}{\partial\alpha^2} = 4\,\cos(2\alpha + \gamma) \quad \frac{\partial^2\psi}{\partial\alpha^2} = 4\,\cos(i\pi) \tag{56}$$

Therefore, odd values of i result in maxima, whereas even values result in minima, and the required spacecraft orientation for increasing or decreasing the semimajor axis is specified by Eq. (57):

$$\alpha = \begin{cases} -\frac{\gamma}{2} + \frac{\pi}{2}, & \dot{a} > 0 \\ -\frac{\gamma}{2}, & \dot{a} < 0 \end{cases} \tag{57}$$

By maintaining a spacecraft orientation according to Eq. (57), the rate of change of the semimajor axis may be maximized or minimized to provide the greatest propulsive effect for raising or lowering the orbit. Further analysis of Eq. (52) shows that the dependence upon the ratio a/r and speed v means the effect will be greater at periapsis during an eccentric orbit. There is also a dependence upon the square of the ratio λ, which highlights the fact that a larger spacecraft will generate an even greater effect accordingly. Figure 4 shows the angle α required for increasing or decreasing the semimajor axis for orbits with various eccentricity values and an initial semimajor axis of 7000 km.

B. Eccentricity

The eccentricity of the orbit is determined from Eq. (58), where $h = r^2\dot{\theta}$ is the orbit angular momentum of the spacecraft:

$$e = \sqrt{1 - \frac{h^2}{\mu a}} \quad = \sqrt{1 - \frac{r^4\dot{\theta}^2}{\mu a}} \tag{58}$$

Differentiation of Eq. (58) in time results in Eq. (59), which is the rate of change of the eccentricity:

$$\dot{e} = \frac{1}{2e}\left(-\frac{4r^3\dot{r}\dot{\theta}^2}{\mu a} - \frac{2r^4\dot{\theta}\ddot{\theta}}{\mu a} + \frac{r^4\dot{\theta}^2}{\mu a^2}\dot{a}\right) \tag{59}$$

Substitution of Eqs. (19) and (50) for the $\ddot{\theta}$ and $\dot{a}$ terms, respectively, results in Eq. (60). Note that Eq. (58) has also been rearranged and substituted within the final term:

$$\dot{e} = \frac{1}{ea}\left[-r\dot{\theta}\eta\lambda\Delta s_\alpha + (1 - e^2)\left(\frac{a}{r}\right)^2\dot{r}(1 - \beta)\right.$$
$$\left. + (1 - e^2)\left(\frac{a}{r}\right)^2\eta\lambda\Delta(\dot{r}c_\alpha + r\dot{\theta}s_\alpha)\right] \tag{60}$$

Further substitution of the velocity components in terms of speed v and flight-path angle γ, as well as the definition of $\rho = (1 - e^2)(a/r)^2$, results in Eq. (61):

$$\dot{e} = \frac{v}{ea}[(\rho - 1)\eta\lambda\Delta s_\gamma s_\alpha + \rho\eta\lambda\Delta c_\gamma c_\alpha + \rho(1 - \beta)c_\gamma] \tag{61}$$

The simplified expressions for Δ and β may then be substituted to yield Eq. (62):

$$\dot{e} = \frac{3\eta\lambda^2 v}{ea}[(\rho - 1)s_\gamma s_\alpha c_\alpha - \rho c_\gamma c_\alpha^2]$$
$$= \frac{3\eta\lambda^2 v}{2ea}[(\rho - 1)s_\gamma s_{2\alpha} - \rho c_\gamma c_{2\alpha} - \rho c_\gamma]$$
$$= \frac{3\eta\lambda^2 v}{2ea}\chi \tag{62}$$

Similar to ψ defined for the rate of change of the semimajor axis, the value of χ must also be maximized or minimized to achieve the greatest possible rate of change of eccentricity. Equations (63–68) define the spacecraft orientation α, which maximizes or minimizes the rate of change:

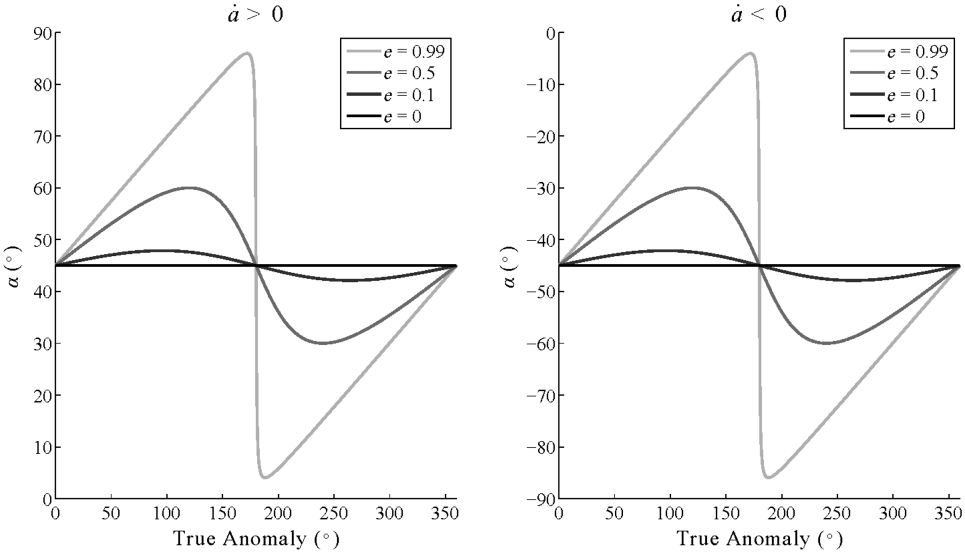

Fig. 4 Required spacecraft orientation for increasing (left) or decreasing (right) the semimajor axis throughout the orbit.

$$\frac{\partial \chi}{\partial \alpha} = 2(\rho - 1)\sin\gamma\cos 2\alpha + 2\rho\cos\gamma\sin 2\alpha$$
$$0 = 2(\rho - 1)\sin\gamma\cos 2\alpha + 2\rho\cos\gamma\sin 2\alpha$$
$$0 = (\rho - 1)\tan\gamma + \rho\tan 2\alpha \tag{63}$$

$$\tan 2\alpha = \frac{1-\rho}{\rho}\tan\gamma \tag{64}$$

$$\alpha = \frac{1}{2}\tan^{-1}\left(\frac{1-\rho}{\rho}\tan\gamma\right) + \frac{\pi}{2}i \tag{65}$$

To handle the quadrant change when the radial component of velocity is positive or negative, the maximum and minimum value of α must be computed using the conditions described in Eqs. (66) and (67), respectively:
Increasing e:

$$\alpha = \begin{cases} \xi - \frac{\pi}{2}, & \cos\gamma \geq 0 \\ \xi, & \cos\gamma < 0 \end{cases} \tag{66}$$

Decreasing e:

$$\alpha = \begin{cases} \xi, & \cos\gamma \geq 0 \\ \xi + \frac{\pi}{2}, & \cos\gamma < 0 \end{cases} \tag{67}$$

where the angle ξ is defined by Eq. (68):

$$\xi = \frac{1}{2}\tan^{-1}\left(\frac{1-\rho}{\rho}\tan\gamma\right) \tag{68}$$

Figure 5 shows the angle α required for increasing or decreasing the eccentricity for orbits with various eccentricities.

C. Apoapsis and Periapsis

The apoapsis r_a and periapsis r_p of the spacecraft orbit are determined from Eqs. (69) and (70), respectively:

$$r_a = a(1+e) \tag{69}$$

$$r_p = a(1-e) \tag{70}$$

Differentiating in time, the rate of change of the apoapsis and periapsis are determined from Eqs. (71) and (72), respectively:

$$\dot{r}_a = \dot{a}(1+e) + a\dot{e} \tag{71}$$

$$\dot{r}_p = \dot{a}(1-e) - a\dot{e} \tag{72}$$

To increase or decrease the apoapsis while maintaining a constant periapsis, or vice versa, the value of $\dot{r}_a$ or $\dot{r}_p$ may be set to zero. The combination of Eqs. (71) and (72) under such a condition results in the relationships given by Eqs. (73) and (74), where the former is for changing only the apoapsis and the latter for changing only the periapsis:

$$0 = \dot{a}(1-e) - a\dot{e} \tag{73}$$

$$0 = \dot{a}(1+e) + a\dot{e} \tag{74}$$

Equations (50) and (61) may be substituted into Eqs. (73) and (74) to yield the relationships given by Eqs. (75) and (76) for apoapsis and periapsis control, respectively:

$$0 = z_a(1-\beta) + \eta\lambda\Delta[(z_a - 1)s_\gamma s_\alpha + z_a c_\gamma c_\alpha] \tag{75}$$

$$0 = z_p(1-\beta) + \eta\lambda\Delta[(z_p - 1)s_\gamma s_\alpha + z_p c_\gamma c_\alpha] \tag{76}$$

where the normalized apoapsis and periapsis parameters z_a and z_p are defined by Eqs. (77) and (78):

$$z_a = (1-e)^2\left(\frac{a}{r}\right)^2 \tag{77}$$

$$z_p = (1+e)^2\left(\frac{a}{r}\right)^2 \tag{78}$$

The simplified expressions for Δ and β may then be substituted to yield Eq. (79), where $z = z_a$ for apoapsis control and $z = z_p$ for periapsis control:

$$0 = c_\alpha[(z-1)s_\gamma s_\alpha - z c_\gamma c_\alpha] \tag{79}$$

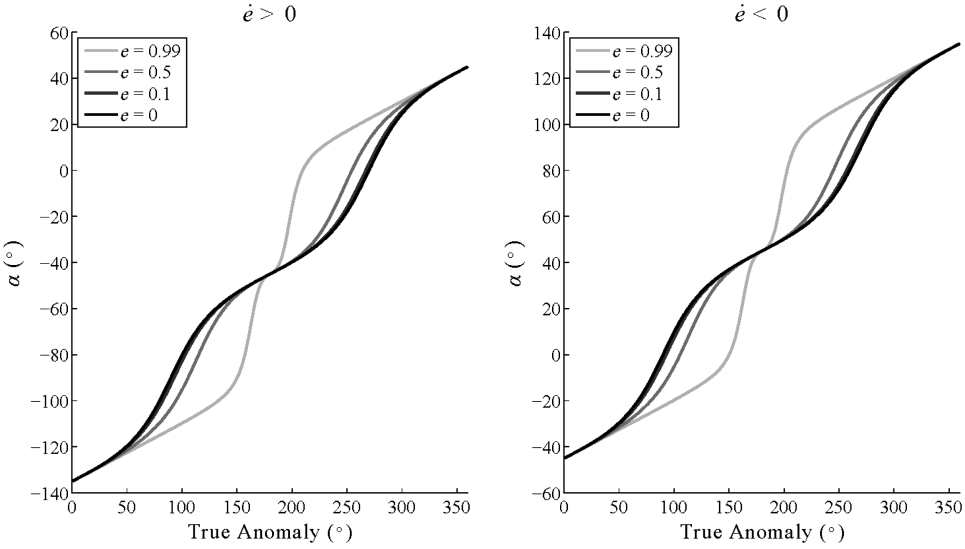

Fig. 5 Required spacecraft orientation for increasing (left) or decreasing (right) the eccentricity throughout the orbit.

There is a trivial solution at $\alpha = \pm\pi/2$, whereas Eqs. (80–82) define the nontrivial solution:

$$0 = (z-1)s_\gamma s_\alpha - z c_\gamma c_\alpha \tag{80}$$

$$0 = (z-1)\tan\gamma\tan\alpha - z \tag{81}$$

$$\alpha = \tan^{-1}\left(\frac{z}{z-1}\cot\gamma\right) \tag{82}$$

The nontrivial solution corresponds to increasing and decreasing the apsis. During one-half of the orbit, the apsis will be increased, and during the other half, the apsis will be decreased. Therefore, the spacecraft orientation must follow the nontrivial solution during the appropriate half of the orbit and the trivial solution during the other half. Equations (83–86) define the required orientation for raising and lowering the apoapsis and periapsis accordingly.

Raising apoapsis:

$$\alpha = \begin{cases} \zeta, & \cos\gamma \geq 0 \\ \frac{\pi}{2}, & \cos\gamma < 0 \end{cases} \tag{83}$$

Lowering apoapsis:

$$\alpha = \begin{cases} -\frac{\pi}{2}, & \cos\gamma \geq 0 \\ \zeta, & \cos\gamma < 0 \end{cases} \tag{84}$$

Raising periapsis:

$$\alpha = \begin{cases} \frac{\pi}{2}, & \cos\gamma \geq 0 \\ \zeta, & \cos\gamma < 0 \end{cases} \tag{85}$$

Lowering periapsis:

$$\alpha = \begin{cases} \zeta, & \cos\gamma \geq 0 \\ -\frac{\pi}{2}, & \cos\gamma < 0 \end{cases} \tag{86}$$

where the angle ζ is defined by Eq. (87), with the appropriate value of z used for apoapsis or periapsis control:

$$\zeta = \tan^{-1}\left(\frac{z}{1-z}\cot\gamma\right) \tag{87}$$

Figure 6 shows the angle α required for increasing or decreasing the apoapsis for orbits with various eccentricities, and Fig. 7 shows the required angle for increasing or decreasing the periapsis.

D. Argument of Periapsis

The radial location of the spacecraft r is defined by Eq. (88) in terms of the orbital parameters and angular location θ, where ω is the argument of periapsis:

$$r = \frac{a(1-e^2)}{1 + e\cos(\theta-\omega)} \tag{88}$$

Differentiating in time results in Eq. (89):

$$\dot{r} = \frac{e r^2\dot{\theta}}{a(1-e^2)}\sin(\theta-\omega) \tag{89}$$

By combining Eqs. (88) and (89), the argument of periapsis may be determined from Eq. (90), where $p = a(1-e^2)$ is the semilatus rectum:

$$\omega = \theta - \tan^{-1}\left[\frac{p\left(\frac{\dot{r}}{r\dot{\theta}}\right)}{p-r}\right] \tag{90}$$

The rate of change of the argument of periapsis is then determined by differentiating Eq. (90) by time, which results in Eq. (91):

$$\dot{\omega} = \dot{\theta} - \frac{\Theta}{(p-r)^2 v^2 s_\gamma^2 + p^2 v^2 c_\gamma^2} \tag{91}$$

where the parameter Θ is defined by Eq. (92).

$$\begin{aligned}\Theta = {} & p(p-r)\left[\frac{v^3}{r}s_\gamma^3 - v s_\gamma \frac{\mu}{r^2}\left(1 + \frac{3}{2}\eta\lambda^2\right)\right] \\ & - \frac{3}{2}p(p-r)\frac{\mu}{r^2}v\eta\lambda^2(s_\gamma c_{2\alpha} + c_\gamma s_{2\alpha}) \\ & + p^2\frac{v^3}{r}s_\gamma c_\gamma^2 - 3rv^3 s_\gamma^2 c_\gamma \eta\lambda^2 s_{2\alpha}\end{aligned} \tag{92}$$

To change the argument of periapsis, the spacecraft orientation must be controlled to maximize or minimize Θ. Equations (93–96) define the appropriate spacecraft orientation:

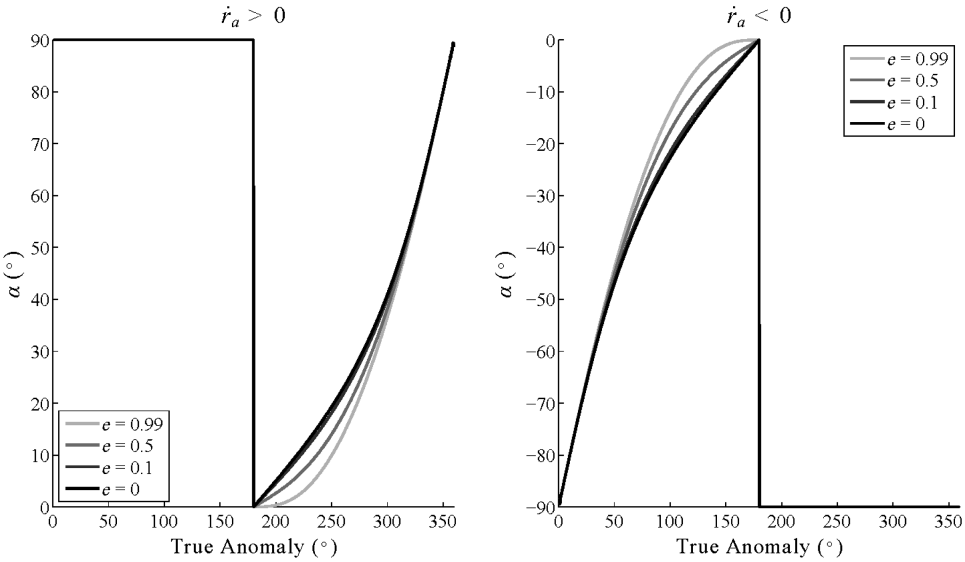

Fig. 6 Required spacecraft orientation for increasing (left) or decreasing (right) the apoapsis throughout the orbit.

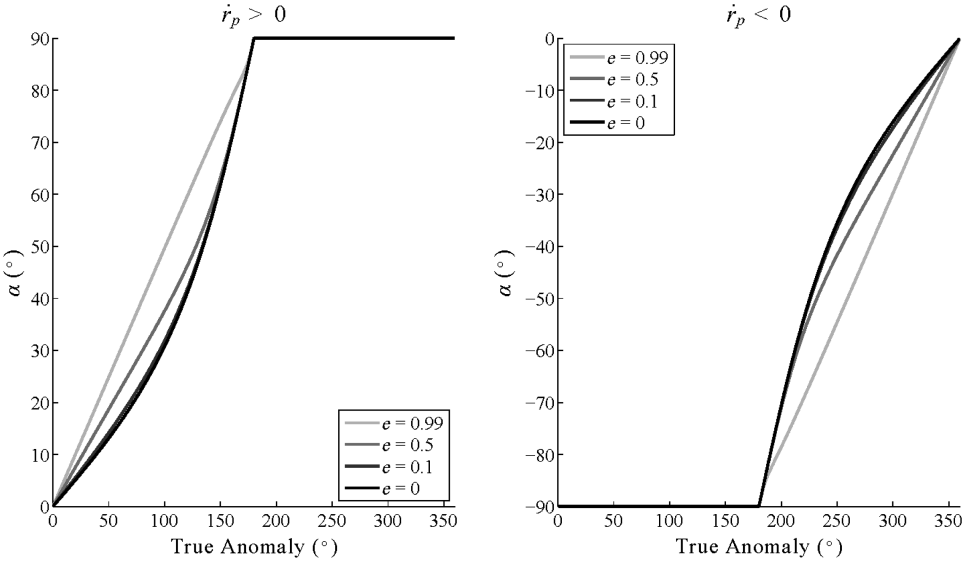

Fig. 7 Required spacecraft orientation for increasing (left) or decreasing (right) the periapsis throughout the orbit.

$$\frac{\partial \Theta}{\partial \alpha} = 3p\frac{\mu}{r^2}\eta\lambda^2 v[(p-r)s_\gamma s_{2\alpha} - (p+r)c_\gamma c_{2\alpha}] \tag{93}$$

$$0 = (p-r)s_\gamma s_{2\alpha} - (p+r)c_\gamma c_{2\alpha} \tag{94}$$

$$0 = (p-r)\tan\gamma\,\tan 2\alpha - (p+r) \tag{95}$$

$$\alpha = \frac{1}{2}\tan^{-1}\left(\frac{p+r}{p-r}\cot\gamma\right) \tag{96}$$

Increasing or decreasing the argument of periapsis may be accomplished by setting the spacecraft orientation according to Eq. (97) or (98), respectively:

Increasing ω:

$$\alpha = \begin{cases} \sigma, & p-r \geq 0 \\ \sigma + \frac{\pi}{2}, & p-r < 0 \end{cases} \tag{97}$$

Decreasing ω:

$$\alpha = \begin{cases} \sigma + \frac{\pi}{2}, & p-r \geq 0 \\ \sigma + \pi, & p-r < 0 \end{cases} \tag{98}$$

where the angle σ is defined by Eq. (99):

$$\sigma = \frac{1}{2}\tan^{-1}\left(\frac{p+r}{p-r}\cot\gamma\right) \tag{99}$$

Figure 8 shows the angle α required for increasing or decreasing the argument of periapsis for orbits with various eccentricities.

E. Summary

The required spacecraft orientation has been determined for orbit maneuvers that change the semimajor axis, eccentricity, apoapsis, periapsis, and argument of periapsis. By maintaining the orientation specified by the appropriate functions of the orbital elements and flight-path angle, thrust from the tangential component of gravitational forces is generated, which maximizes the change in each parameter. The specified orientation angle α for each type of maneuver is summarized in Table 1 and Eqs. (100–102):

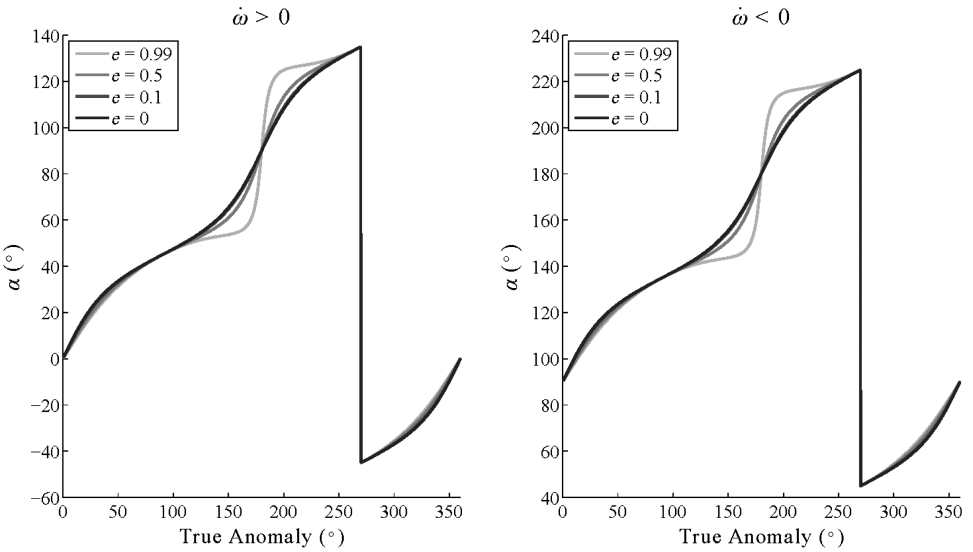

Fig. 8 Required spacecraft orientation for increasing (left) or decreasing (right) the argument of periapsis throughout the orbit.

Table 1 Summary of required spacecraft orientation angles for various orbit maneuvers

	Spacecraft orientation, α			
	Increase		Decrease	
Parameter	$\cos\gamma \geq 0$	$\cos\gamma < 0$	$\cos\gamma \geq 0$	$\cos\gamma < 0$
a	$-\frac{\gamma}{2}+\frac{\pi}{2}$		$-\frac{\gamma}{2}$	
e	$\xi-\frac{\pi}{2}$	ξ	ξ	$\xi+\frac{\pi}{2}$
r_a	$\frac{\pi}{2}$	ζ_a	ζ_a	$-\frac{\pi}{2}$
r_p	ζ_p	$\frac{\pi}{2}$	$-\frac{\pi}{2}$	ζ_p
ω	$\sigma+\frac{\pi}{2}$		σ	

$$\xi = \frac{1}{2}\tan^{-1}\left(\frac{1-\rho}{\rho}\tan\gamma\right) \tag{100}$$

$$\zeta = \tan^{-1}\left(\frac{z}{1-z}\cot\gamma\right) \tag{101}$$

$$\sigma = \frac{1}{2}\tan^{-1}\left(\frac{p+r}{p-r}\cot\gamma\right) \tag{102}$$

F. Energy Balance

To change the orbit of the spacecraft, there must be energy input to the system. Mechanical work is performed by the spacecraft attitude control system to maintain the desired orientation, providing the required energy input. Equation (103) shows the orbit energy of the spacecraft, which is described in terms of the semimajor axis:

$$E = \frac{-\mu M_T}{2a} \tag{103}$$

The rate of change of the orbital energy is described by Eq. (104), which is determined by differentiation of Eq. (103) with respect to time:

$$\dot{E} = \frac{\mu M_T}{2a^2}\dot{a} \tag{104}$$

The mechanical power provided by the attitude control system P_ϕ is described by the product of the input torque Q_ϕ and orientation rate of change $\dot{\phi}$ as shown in Eq. (105):

$$P_\phi = Q_\phi\dot{\phi} \quad = M_T\eta\left(L^2\ddot{\phi} + \frac{\mu}{r^2}L\Delta\,\sin\alpha\right)\dot{\phi} \tag{105}$$

Therefore, integration of Eq. (105) results in the energy input to the system, which balances the change in orbit energy. As an example, consider the spacecraft in a circular orbit, where the following conditions apply: $e = 0$, $a = r$, $\gamma = \pi/2$, $\alpha = \pi/4$, $\dot{\phi} = \dot{\theta}$, and $\ddot{\phi} = 0$. Substitution of these conditions, as well as the simplified expression for Δ, results in Eq. (106):

$$\begin{aligned} P_\phi &= M_T\eta\left(L^2\ddot{\phi} + \frac{\mu}{r^2}L\Delta\,\sin\alpha\right)\dot{\phi} \\ &= 3M_T\eta\lambda^2\frac{\mu}{a}\dot{\theta}\,\sin\alpha\,\cos\alpha \\ &= \frac{3}{2}M_T\eta\lambda^2\frac{\mu}{a}\dot{\theta} \end{aligned} \tag{106}$$

Because the orbit is circular, the angular rate $\dot{\theta}$ may be determined from Eq. (107):

$$\dot{\theta} = \sqrt{\frac{\mu}{a^3}} \tag{107}$$

Substitution of Eq. (107) within Eq. (106) results in Eq. (108):

$$P_\phi = \frac{3}{2}M_T\eta\lambda^2\sqrt{\frac{\mu^3}{a^5}} \tag{108}$$

Considering the rate of change of the orbital energy described by Eq. (104), the expression for $\dot{a}$ may be substituted from Eq. (52) and simplified according to the conditions for circular orbit. This results in Eq. (110), where the spacecraft speed v is determined by Eq. (109):

$$v = \sqrt{\frac{\mu}{a}} \tag{109}$$

$$\begin{aligned} \dot{E} &= \frac{\mu M_T}{2a^2}\left[3\left(\frac{a}{r}\right)^2\eta\lambda^2 v\psi\right] \\ &= \frac{3}{2}\frac{\mu M_T}{a^2}\eta\lambda^2\sqrt{\frac{\mu}{a}} \\ &= \frac{3}{2}M_T\eta\lambda^2\sqrt{\frac{\mu^3}{a^5}} \end{aligned} \tag{110}$$

Equation (110) is identical to Eq. (108), verifying the energy balance between the mechanical work input and spacecraft orbital energy.

G. Angular Momentum Balance

Maintaining the specified spacecraft orientation requires torque input by the attitude control system, which results in angular momentum transferred between the attitude control system and the spacecraft orbit. The angular momentum of the spacecraft is described by Eq. (111):

$$H = M_T r^2\dot{\theta} \tag{111}$$

Differentiating Eq. (111) by time, the rate of change of the orbit angular momentum is described by Eq. (112):

$$\begin{aligned} \dot{H} &= M_T(2r\dot{r}\,\dot{\theta} + r^2\ddot{\theta}) \\ &= \frac{M_T\mu\eta\lambda}{r}\Delta\,\sin\alpha \\ &= \frac{3}{2}\frac{M_T\mu\eta\lambda^2}{r}\sin 2\alpha \end{aligned} \tag{112}$$

Assuming the simplified conditions for semimajor axis control while the spacecraft is in circular orbit, where $\alpha = \pi/4$, the rate of change of orbit angular momentum is given by Eq. (113):

$$\dot{H} = \frac{3}{2}\frac{M_T\mu\eta\lambda^2}{r} \tag{113}$$

Under the same conditions, the torque applied by the attitude control system is determined by Eq. (114):

$$\begin{aligned} Q_\phi &= M_T\eta\left(L^2\ddot{\phi} + \frac{\mu}{r^2}L\Delta\,\sin\alpha\right) \\ &= \frac{M_T\mu\eta\lambda\Delta}{r}\sin\alpha \\ &= \frac{3}{2}\frac{M_T\mu\eta\lambda^2}{r} \end{aligned} \tag{114}$$

Because Eq. (114) is identical to Eq. (113), the change in orbit angular momentum of the spacecraft is balanced by the torque input due to the attitude control system.

H. Application

One of the benefits of this type of propulsion method is that it may be applied using any spacecraft that is equipped with an active attitude control system (or other actuators able to generate torque). This is because thrust is generated based upon the distribution of mass across the volume of the spacecraft and its orientation with respect to the central body. The equations of motion would have to be reexamined to model the actual propulsive thrust due to the gravitational gradient upon a continuous distribution of mass. However, a preliminary estimation of the thrust upon a continuous spacecraft is performed by determining an equivalent dumbbell model given the inertial parameters of the vehicle. Note that this equivalent model assumes mass is concentrated purely along the longitudinal axis of the vehicle. In fact, mass distributed across the lateral axis of the vehicle will produce a counteractive thrust due to its perpendicular alignment with respect to the zenith. Therefore, the dumbbell model is expected to overestimate the amount of propulsive thrust generated.

Recall that the dumbbell model consists of a spacecraft composed of two masses m and M, separated by a rigid link of length L, and with a mass ratio of ε, which also dictates the location of the center of mass along the rigid link. Therefore, the equivalent total mass M_T, length L, and mass ratio ε must be determined for a spacecraft with continuous volume. The total mass is assumed to be equal to the given spacecraft mass, whereas the equivalent length and mass ratio are assumed to be defined by the moment of inertia about an axis perpendicular to the orbit plane I_ϕ. The moment of inertia of the simplified model, given by Eq. (115), is assumed to equal to that of the continuous spacecraft:

$$I_\phi = M_T \eta L^2 \tag{115}$$

The equivalent mass ratio ε is estimated from the given location of the spacecraft center of mass with respect to its overall length (referenced to one end of the vehicle). Therefore, the equivalent length L may be determined by rearranging Eq. (115):

$$L = \sqrt{\frac{I_\phi}{M_T \eta}} \tag{116}$$

Assuming the vehicle is placed in a circular low Earth orbit with an altitude of 450 km, the equivalent propulsive thrust may be determined from Eq. (44). An orientation angle of $\alpha = 45$ deg is used to maximize the propulsive effect, which yields Eq. (117) after substituting Δ:

$$F_\theta = \frac{3}{2}\frac{\mu}{r^2} M_T \eta \lambda^2 \tag{117}$$

Parameters for the space transportation system (STS) orbiter and International Space Station (ISS) are shown in Table 2, including the total mass, estimated mass ratio, moment of inertia, and equivalent length [21]. The resulting propulsive thrust generated due to the gravitational gradient is also shown in Table 2.

Both the orbiter and ISS generate relatively tiny amounts of gravity-induced thrust even with the generous assumptions of the dumbbell model. The thrust generated by the ISS is an order of magnitude larger than that of the orbiter due to the larger values of ε and L. Although this propulsion method would not be applied to either of these vehicles, this analysis serves to provide a baseline example.

Table 2 Inertial parameters for the STS orbiter and ISS [21]

Parameter	Orbiter	ISS
M_T, kg	110,264	212,169
ε	0.33	0.51
I_Ω, kg · m^2	10,829,834	96,950,112
L, m	21.1	42.8
F_θ, μN	3.0	26.7

Table 3 Initial orbital elements used during simulation

Parameter	Value
a	6828 km
e	0.02197
r_a	6978 km
r_p	6678 km
ω	0°

IV. Simulation

The two-body equations of motion are simulated using a Mathworks MATLAB Simulink model with variable time step ODE45 Dormand–Prince solver and a relative tolerance of 10^{-4}. Although the desired spacecraft orientation for most of the analyses is determined using the simplified expressions for Δ and β, simulation of the spacecraft response is performed using the original equations of motion. No perturbations due to atmosphere, gravity harmonics, or other effects are considered.

The spacecraft orientation is controlled with respect to the inertial coordinate frame (the angle ϕ instead of α) using a proportional integral derivative (PID) control law, where the desired orientation is prescribed by the respective angles shown in Table 1.

Each parameter is controlled independently, but some coupling is observed between the various parameters. Although it may be possible to superimpose the desired orientation angles to simultaneously change multiple parameters, that approach is not investigated in this study.

The effects of the proposed propulsion method are emphasized for demonstration using a spacecraft length of 10 km and mass of 100,000 kg, producing exaggerated changes in the orbital elements over a simulation duration of one day. Earth is used as a central body ($\mu = 398,601.2$ km^2/s^2), and the spacecraft is placed in an initial orbit with the conditions shown in Table 3.

Figures 9–13 show the results of simulated control of the spacecraft orientation for increasing the semimajor axis, eccentricity, argument of periapsis, apoapsis, and periapsis. The spacecraft semimajor axis, eccentricity, and argument of periapsis are shown in Figs. 9–11, whereas the apoapsis and periapsis are shown in Figs. 12 and 13.

The results demonstrate the ability to change each parameter by controlling the spacecraft orientation appropriately. Although there is some coupling between the parameters, the effects are relatively small during control of the semimajor axis, eccentricity, and argument of periapsis. However, during control of the apoapsis or periapsis, there is a much more significant coupling between the two parameters. To avoid this effect, the exact solution to Eqs. (73) and (74) may be determined using a numerical search without the assumption of approximated values for Δ and β. Figures 12 and 13 compare the results of using the approximated and exact solutions, where negligible coupling is observed using the latter.

Figure 14 shows the desired and actual spacecraft orientation α during control of the eccentricity. It can be seen that the actual orientation tracks the desired orientation relatively well, with some overshoot at the discontinuities. Although the PID control gains may be tuned to improve the tracking, orientation errors due to the discontinuities do not have a significant adverse effect upon the control of the orbit parameters.

The equations of motion used during simulation are those determined using the Lagrange dynamics approach, which assumes the central body is fixed in inertial coordinates. To validate this assumption, the equations of motion determined using the Newton–Euler dynamics approach are also simulated under the same conditions for comparison. Figure 15 shows the resulting semimajor axis of the spacecraft using each approach, where a negligible difference is observed.

It is important to note that the spacecraft size has been exaggerated to amplify the propulsive effects and result in significant changes for demonstration. Although this paper primarily serves to demonstrate the proposed propulsion method and analyze the equations of

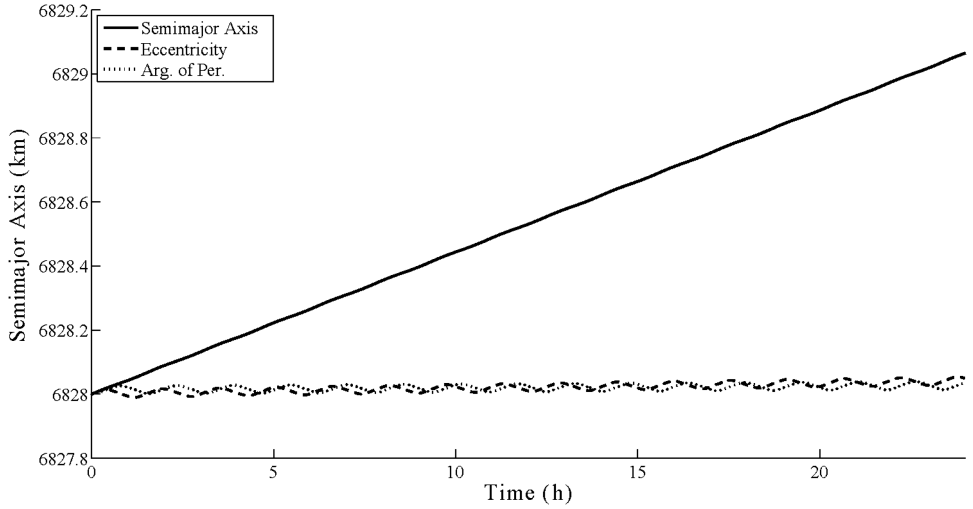

Fig. 9 Resulting semimajor axis of the spacecraft during control of the semimajor axis, eccentricity, and argument of periapsis (Arg. of Per.).

motion, the feasibility of its use in spacecraft of more reasonable sizes must also be addressed. Consider the rate of change of the semimajor axis $\dot{a}$, which may be defined according to Eq. (118):

$$\dot{a} = \frac{3}{4} L^2 \sqrt{\frac{\mu}{r^5}} \tag{118}$$

Larger celestial bodies are expected to generate a greater amount of thrust based on the higher value of μ. However, the ratio λ means that spacecraft of equal sizes will generate higher thrusts around smaller bodies. A number of celestial bodies are considered to establish a trend relating $\dot{a}$ and the sizes of the celestial bodies. Values are computed for each one based on an initial circular orbit with an altitude of 5% of the mean radius. The spacecraft itself is assumed to

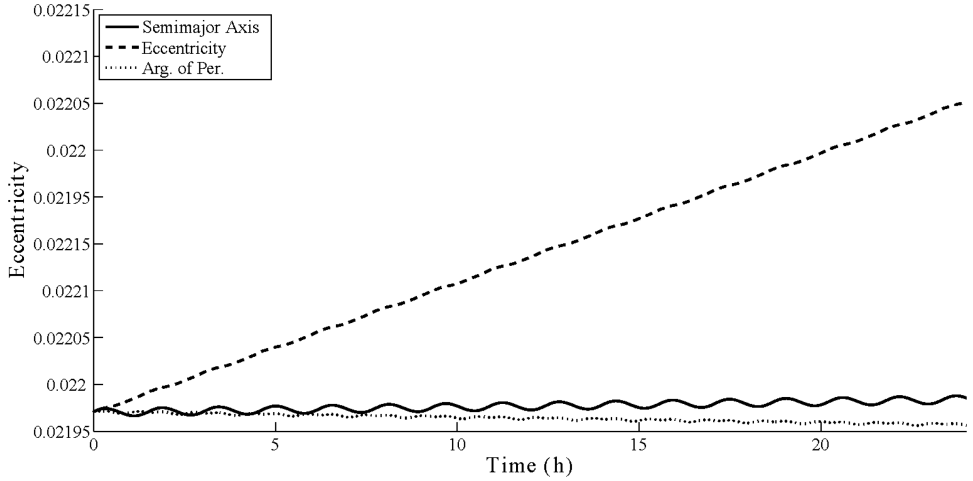

Fig. 10 Resulting eccentricity of the spacecraft during control of the semimajor axis, eccentricity, and argument of periapsis.

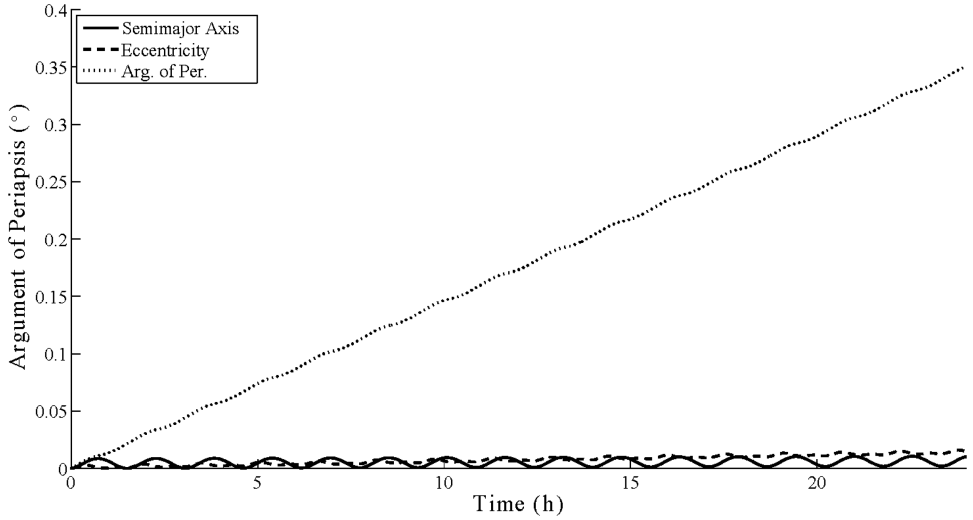

Fig. 11 Resulting argument of periapsis of the spacecraft during control of the semimajor axis, eccentricity, and argument of periapsis.

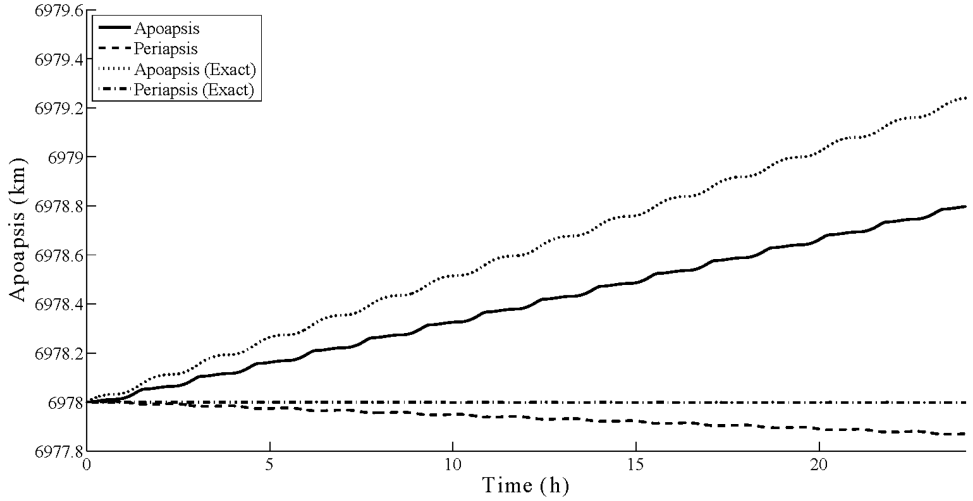

Fig. 12 Resulting apoapsis of the spacecraft during control of the apoapsis and periapsis using both approximate and exact solutions.

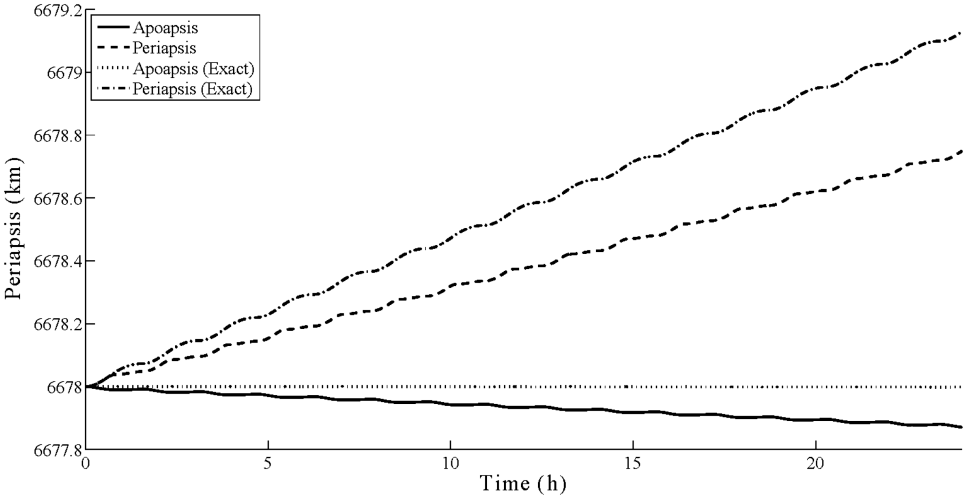

Fig. 13 Resulting periapsis of the spacecraft during control of the apoapsis and periapsis using both approximate and exact solutions.

be 100 m in length. Figure 16 shows the resulting relationship between the mean radius and semimajor axis rate, where both x and y axes are logarithmic.

The relationship between the logarithms of $\dot{a}$ and the mean radius is nearly linear. It is clear that smaller bodies result in significantly higher rates of change for the semimajor axis. Therefore, the proposed method is applied to a spacecraft departing the asteroid 101955 Bennu, which is being targeted for the planned OSIRIS-REx sample return mission [22]. Assuming a spacecraft of 100 m length, and starting within a circular orbit 100 m above the surface, gravity gradient propulsion may be used to escape into heliocentric orbit after approximately 165 days. Simulation of the maneuver is shown in Fig. 17. Note that the simulation is modified to use a constrained three-body model, where the gravity force from the sun is included

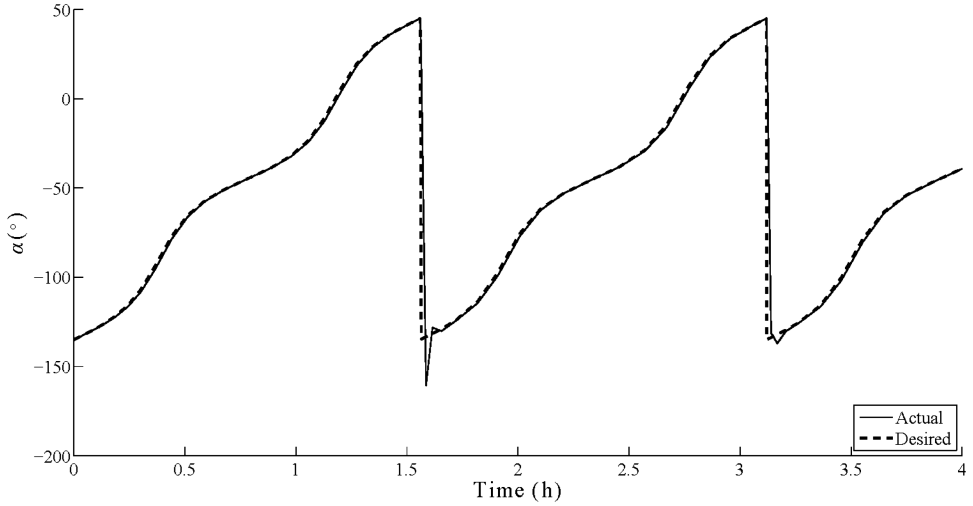

Fig. 14 Desired and actual spacecraft orientation during control of the eccentricity.

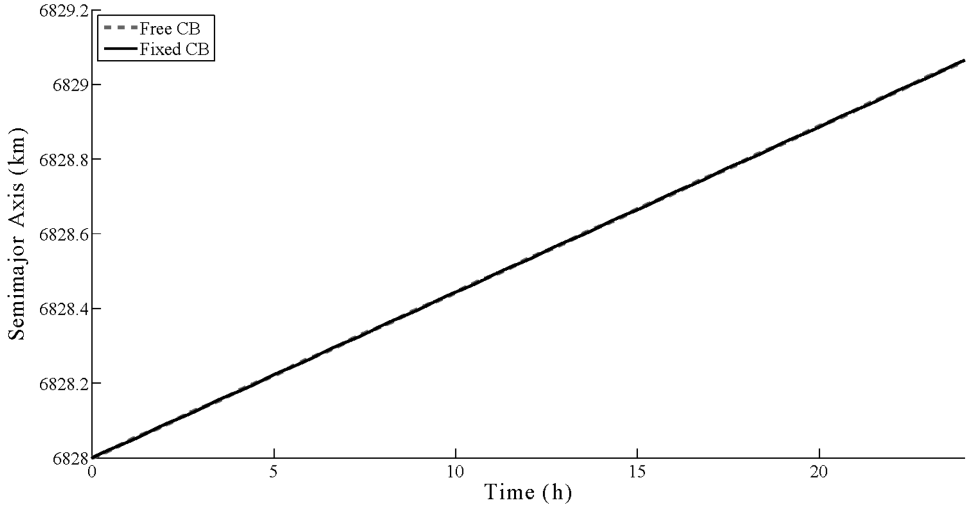

Fig. 15 Comparison of simulation results (semimajor axis) using Lagrange dynamics with a fixed CB and Newton–Euler dynamics with a free CB.

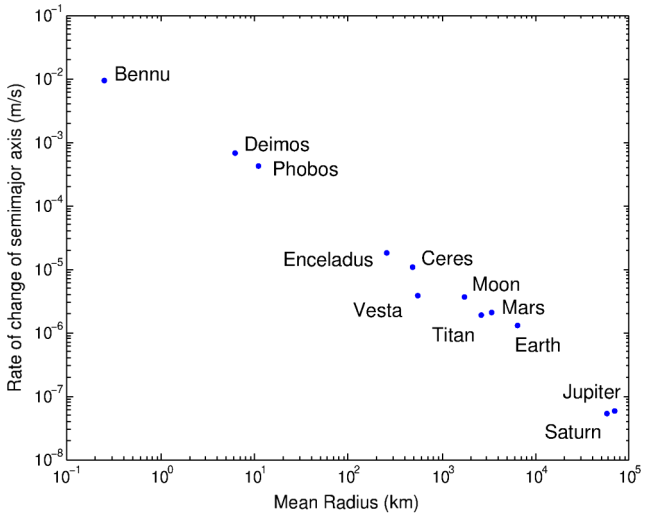

Fig. 16 Rate of change of the semimajor axis about various central bodies.

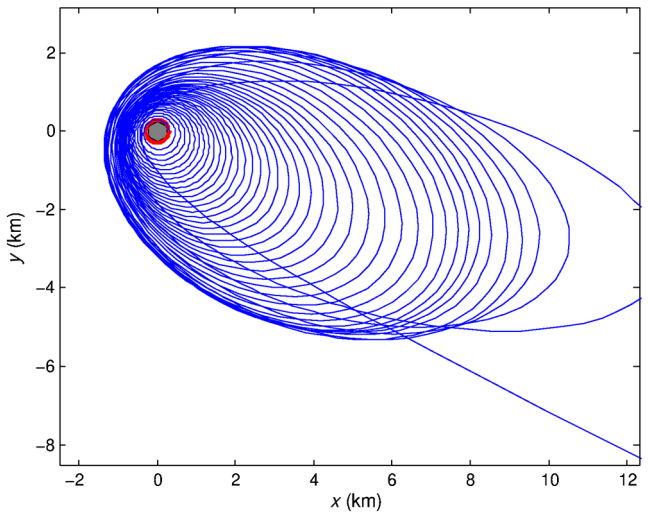

Fig. 17 Resulting trajectory for a spacecraft escaping the asteroid Bennu.

and the asteroid is assumed to stay within its prescribed orbit. For comparison, if the spacecraft length is reduced to 20 m, the maneuver would take approximately 12 years.

V. Conclusions

Spacecraft propulsion has been successfully demonstrated through analysis and simulation by controlling the vehicle orientation to generate thrust due to the effects of the gravitational gradient. Orientation profiles were analytically determined for maximizing the rate of change of the semimajor axis, eccentricity, and argument of periapsis, as well as the apoapsis and periapsis. Energy and angular momentum are input into the system using the attitude control system, which balances the respective changes in orbit energy and angular momentum. Although the effect is small, this technique may be useful for maintaining orbit in the presence of atmospheric drag, transferring to and from asteroids, or possibly to reduce the requirements of a primary propulsion system. Another possible application is the use of this method during a flyby maneuver to gain an additional increase in speed.

References

[1] Johnson, L., "Propulsion Technologies for Exploration of the Solar System and Beyond," *Review of Scientific Instruments*, Vol. 73, No. 2, 2002, p. 1079. doi:10.1063/1.1431426

[2] Wie, B., "Dynamics and Control of Gravity Tractor Spacecraft for Asteroid Deflection," *Journal of Guidance, Control, and Dynamics*, Vol. 31, No. 5, Sept. 2008, pp. 1413–1423. doi:10.2514/1.32735

[3] Neumann, P., Bilek, M., Tarrant, R., and McKenzie, D., "Pulsed Cathodic Arc Spacecraft Propulsion System," *Plasma Sources Science and Technology*, Vol. 18, No. 4, Nov. 2009, Paper 045005. doi:10.1088/0963-0252/18/4/045005

[4] Garulli, A., Giannitrapani, A., Leomanni, M., and Scortecci, F., "Autonomous Low-Earth-Orbit Station-Keeping with Electric Propulsion," *Journal of Guidance, Control, and Dynamics*, Vol. 34, No. 6, Nov. 2011, pp. 1683–1693. doi:10.2514/1.52985

[5] Gangestad, J. W., Pollock, G. E., and Longuski, J. M., "Propellantless Stationkeeping at Enceladus via the Electromagnetic Lorentz Force," *Journal of Guidance, Control, and Dynamics*, Vol. 32, No. 5, Sept. 2009, pp. 1466–1475. doi:10.2514/1.42769

[6] Wong, B., and Damaren, C., "Control of the Electrodynamic Boom Propulsion System Accounting for Atmospheric Drag," *Journal of Guidance, Control, and Dynamics*, Vol. 33, No. 5, Sept. 2010, pp. 1327–1333. doi:10.2514/1.48972

[7] Pardini, C., Hanada, T., and Krisko, P. H., "Benefits and Risks of Using Electrodynamic Tethers to De-Orbit Spacecraft," *Acta Astronautica*, Vol. 64, Nos. 5–6, March 2009, pp. 571–588. doi:10.1016/j.actaastro.2008.10.007

[8] Janhunen, P., "Photonic Spin Control for Solar Wind Electric Sail," *Acta Astronautica*, Vol. 83, No. 1, Feb. 2013, pp. 85–90. doi:10.1016/j.actaastro.2012.10.017

[9] Quarta, A., Mengali, G., and Aliasi, G., "Optimal Control Laws for Heliocentric Transfers with a Magnetic Sail," *Acta Astronautica*,

Vol. 89, No. 1, Aug. 2013, pp. 216–225.
doi:10.1016/j.actaastro.2013.04.018

[10] Doody, D. F., "Aerobraking the Magellan Spacecraft in Venus Orbit," *Acta Astronautica*, Vol. 35, No. 94, Jan. 1995, pp. 475–480.
doi:10.1016/0094-5765(94)00214-7

[11] Zhang, W., Han, B., and Zhang, C., "Spacecraft Aerodynamics and Trajectory Simulation During Aerobraking," *Applied Mathematics and Mechanics*, Vol. 31, No. 9, Sept. 2010, pp. 1063–1072.
doi:10.1007/s10483-010-1342-x

[12] Lambert, C., Kumar, B. S., Hamel, J.-F., and Ng, A., "Implementation and Performance of Formation Flying Using Differential Drag," *Acta Astronautica*, Vol. 71, No. 1, Feb. 2011, pp. 68–82.
doi:10.1016/j.actaastro.2011.08.013

[13] Murray, C., and Cartmell, M. P., "Moon-Tracking Orbits Using Motorized Tethers for Continuous Earth-Moon Payload Exchanges," *Journal of Guidance, Control, and Dynamics*, Vol. 36, No. 2, March 2013, pp. 567–576.
doi:10.2514/1.56248

[14] Zimmermann, F., Schöttle, U. M., and Messerschmid, E., "Optimization of the Tether-Assisted Return Mission of a Guided Re-Entry Capsule," *Aerospace Science and Technology*, Vol. 9, No. 8, Nov. 2005, pp. 713–721.
doi:10.1016/j.ast.2005.09.002

[15] Williams, P., "Dynamics and Control of Spinning Tethers for Rendezvous in Elliptic Orbits," *Journal of Vibration and Control*, Vol. 12, No. 7, July 2006, pp. 737–771.
doi:10.1177/1077546306065710

[16] Rudd, R. P., Hall, J. C., and Spradlin, G. L., "Voyager Interstellar Mission," *Acta Astronautica*, Vol. 40, Nos. 2–8, 1997, pp. 383–396.
doi:10.1016/S0094-5765(97)00146-X

[17] Si Mohammed, M., Benyettou, M., Bentoutou, Y., Boudjemai, A., Hashida, Y., and Sweeting, M. N., "Three-Axis Active Control System for Gravity Gradient Stabilised Microsatellite," *Acta Astronautica*, Vol. 64, Nos. 7–8, April 2009, pp. 796–809.
doi:10.1016/j.actaastro.2008.12.010

[18] Landis, G., "Reactionless Orbital Propulsion Using Tether Deployment," *Acta Astronautica*, Vol. 26, No. 5, May 1992, pp. 307–312.
doi:10.1016/0094-5765(92)90076-U

[19] Djebli, A., and Pascal, M., "New Method for the Orbital Modification of a Tether Connected Satellite System," *Acta Mechanica*, Vol. 167, Nos. 1–2, Jan. 2004, pp. 113–122.
doi:10.1007/s00707-003-0024-7

[20] Watanabe, Y., and Nakamura, Y., "Orbit Control for a Spacecraft via the Gravity Gradient Force," *Proceedings of the 49th International Astronautical Congress*, Paper IAF-1998-A.2.08, International Astronautical Federation, Paris, 1998.

[21] Posey, J. D., Segun, T. J., and Farrell, T. L., "International Space Station: On-Orbit Assembly, Modeling, and Mass Properties Data (JSC 26557 Revision P)," NASA Technical Rept., NASA Johnson Space Center, 2002.

[22] Chesley, S., Farnocchia, D., Nolan, M., Vokrouhlicky, D., Chodas, P., Milani, A., Spoto, F., Rozitis, B., Benner, L., Bottke, M., Busch, W., Emery, J., Howell, E., Lauretta, D., Margot, J. L., and Taylor, P., "Orbit and Bulk Density of the OSIRIS-REx Target Asteroid (101955) Bennu," *Icarus*, Vol. 235, No. 1, 2014, pp. 5–22.
doi:10.1016/j.icarus.2014.02.020

M. Xin
Associate Editor